Journal of Photochemistry and Photobiology A: Chemistry 204 (2009) 25–31

Contents lists available at ScienceDirect

Journal of Photochemistry and Photobiology A: Chemistry

journal homepage: www.elsevier.com/locate/jphotochem

Isomorphous substitution of Fe in the framework of aluminosilicate MFI by hydrothermal synthesis and their evaluation in *p*-nitrophenol degradation

Ibraheem O. Ali*, Ali M. Ali, Salah M. Shabaan, Karam Seif El-Nasser

Department of Chemistry, Faculty of Science, Al-Azhar University, Nasr City 11884, Cairo, Egypt

ARTICLE INFO

Article history:
Received 24 October 2008
Received in revised form 29 January 2009
Accepted 6 February 2009
Available online 21 February 2009

Keywords:
ZSM-5
TPABr template
Rice husk ash
Fe-ZSM-5
p-Nitrophenol
Characterization
XRD
FT-IR
Surface texturing

ABSTRACT

Raw rise husks (white particles) were used to produce silica through submission to consecutive chemical treatment using NaOH and HCl solutions. The prepared silica was well incorporated with other components under hydrothermal conditions to synthesize ZSM-5. Fe framework-substituted ZSM-5 with constant Si/(Fe + Al) ratios have been synthesized hydrothermally and characterized by physicochemical methods, e.g. X-ray diffraction (XRD), FI-IR, UV–vis spectroscopy and N_2 adsorption. IR spectroscopy of Fe-substituted ZSM-5 shows a new band at 656 cm^{-1} due to Si–O–Fe group supporting framework incorporation. The replacement of Al^{3+} by Fe^{3+} causes a shift of Si–O–T vibration to lower wavenumbers. The presence of tetrahedral Fe^{3+} has been confirmed by XRD and UV–vis spectroscopy. The photocatalytic activity of Fe incorporated ZSM-5 zeolite towards degradation of *p*-nitrophenol (PNP) was well investigated at the atmospheric pressure, 25 °C, with H_2O_2 as an oxidizing agent. The enhanced photocatalytic activity of 0.4FeZ is attributed to charge-transfer excited complex between Fe in zeolite along with PNP ligand in addition to higher surface area and high dispersion Fe in framework comparatively. More information on local structures of metal oxides inside zeolites and their photocatalytic activities towards PNP were deduced, correlated and discussed.

1. Introduction

The isomorphous replacement of aluminum in the zeolite framework by other heteroatoms to prepare metalosilicates having new physicochemical and catalytic properties is an important research subject in the field of zeolite chemistry [1,2]. Incorporation of transition metal ions into the framework creates isolated redox active centers in an ordered matrix. Coordination and stabilization of transition metal ions by the zeolite lattice can significantly affect their catalytic behavior and may lead to catalysts with new and often improved properties [3]. For a steady insertion into a tetrahedral site of zeolite lattice, a heteroelement must obey a certain number of theoretical rules, such as Pauling's first rule requiring a specific range for the ratio of the ionic between M^{n+} and O^{2-} [4–6]. Exceptions may be observed for frameworks that tolerate mixed iono-covalent bondings. Other requirements for a true substitution imply some flexibility of the heteroelements to accept the tetrahedral coordination and an oxidation state compatible with the overall (stable) framework charge [7]. Some elements that have, for example, the appropriate size (ionic radius) required for a stable tetrahedral coordination, are potential candidates or an extended incorporation. This is obviously the case of Al but also for Ge and, to a lesser extent, Be, Ga, Fe and B. Other more bulky elements like Zr, V, Cr, Mo, Sn, In, Zn or even Ti are less readily accommodated in tetrahedral sites [8–11].

Isomorphous substitution of Fe into the zeolite framework has recently attracted increasing interest due to its unique and wide range applications in catalysis [12,13], e.g. the methanol oxidation [14], the oxidative dehydrogenation of propane [15] and the decomposition of *n*-butane [16] and of N_2O in the absence of any reducing agent [17].

In fact Kharitonov and co-workers reported that MFI type ferrisilicate shows higher activity and selectivity than supported oxides of V, Mo, W and Fe in one-step oxidation of benzene to phenol with N_2O [18,19]. They proposed a novel ability of the tetrahedral Fe ions producing specific active sites [18,19]. Lobree et al. have reported that at loadings below Fe/Al = 0.56, Fe^{3+} cations exchange on a one-to-one basis with Brønsted acid protons, but at higher Fe/Al ratios, small particles of Fe_2O_3 particles appear to form [20]. Sachtler and co-workers have reported similar findings [21]. On the other hand, Benjamin et al. the extra-framework iron species in FeMFI prepared via an *ex*-framework route are essential for the formation of reactive oxygen species in direct catalytic decomposition of N_2O, while Lewis or Brønsted acid sites play a minor role in this reaction [22].

In this study, ZSM-5 have been synthesized using rise husk ash and modified by replacement Fe instead of Al. The effect of this substitution on ZSM-5 structure was investigated. These pre-

* Corresponding author. Tel.: +20 2 22629357/8; fax: +20 2 22629356.
E-mail address: iotmana@yahoo.com (I.O. Ali).

1010-6030/$ – see front matter © 2009 Elsevier B.V. All rights reserved.
doi:10.1016/j.jphotochem.2009.02.008

pared samples have been characterized by X-ray diffraction, FT-IR, UV–vis and N_2 adsorption. Finally, the catalytic activity of the Fe-substituted samples toward photocatalytic degradation of *p*-nitrophenol was investigated.

PNP was selected, as a model for the photocatalytic oxidation experiments because it is a high toxicity and/or mutagenicity for many living organisms either directly or through some of their catabolic metabolites. Nitrophenols were on the list of United States environmental protection agency as priority pollutants.

2. Experimental

2.1. Materials

The materials used were: rice husks (RHs) powder (prepared in this work), sodium hydroxide pellets (AR 98%), aluminum sulfate [Merck, $Al_2(SO_4)_3{\cdot}16H_2O$], tetrapropylammonium bromide (TPABr, Fluka), *n*-propyl amine (*n*-PA, Merck) iron nitrate [$Fe(NO_3)_3{\cdot}9H_2O$ Merck], *p*-nitrophenol (Merck) and commercial H_2SO_4.

2.1.1. Silica preparation from rice husk

Dry raw rice husks were sieved to eliminate residual rice and clay particles. They were well washed with distilled water, filtered, dried in air, and calcined at 750 °C for 6 h (white ash). 150 ml of 4 M NaOH solution was added to 12 g of calcined RHs and heated under reflux at 90 °C for 12 h. 20 ml of HCl (32%) was added to the aforementioned base dissolved RHs for complete precipitation. RHs were filtered, washed sample repeatedly with deionized water to remove chloride ions and finally dried in an oven at 120 °C for 6 h. The yield of silica in this sample ash was 42%. The chemical composition of rice husk ash is as follows: loss in ignition, 4.71; SiO_2, 90.70;Al_2O_3, 0.13; Fe_2O_3, 0.06; TiO_2, 0.015; CaO, 0.61; MgO, 0.25; Na_2O, 0.09; K_2O, 2.64; P_2O_5, 0.73, all numbers on wt% basis.

2.1.2. Preparation of ZSM-5

The hydrogels of the following oxide molar compositions were prepared for the synthesis of ZSM-5 zeolite; comparable to those can be found elsewhere [23,24], using the following molar ratios:

$$3.12Na_2O : 0.162Al_2O_3 : 6.185SiO_2 : 0.185TPABr : 100H_2O$$

A specific amount of NaOH was added to silica resulted from rice husk, in a small amount of H_2O (~40 ml) while stirring, followed by heating at 80 °C until a clear solution was reached. TPABr, on the other hand, was dissolved in a little amount of H_2O (10 ml) under heating at 50 °C for 20 min. The solution of TPABr was added to sodium silicate solution with stirring for 15 min. *n*-Propyl amine (1 ml) was added as a mobilizing agent [7]. The combined solution of sodium silicate and TPABr was added to a clear solution of aluminum sulfate (prepared by dissolving 0.5 g of aluminum sulfate in 10 ml of distilled water and 0.05 ml of concentrated H_2SO_4) with stirring for 30 min.

The pH of the mixture was adjusted at 11 by using NaOH (0.1 M) and H_2SO_4 (0.1 M) solutions. Finally, the mixture was hydrothermally treated at 150 °C in an oil bath, using stainless steel autoclaves, for 8 days. The autoclaves were removed at the specified time from the oil bath and quenched immediately with cold water. The solid product was filtered and washed with distilled water until the pH of the filtrate dropped to 8. The products were dried at 110 °C for 10 h, and then calcined at 550 °C for 6 h in an air oven. This sample was denoted as ZSM-5.

2.1.3. Preparation of Fe-ZSM-5 (built-in)

The synthesis procedure is described in molar ratio as follows:

$$3 : 12Na_2O : (1-x)Al_2O_3 : xFe_2O_3 : 6.185SiO_2 : 0.185TPABr : 100H_2O$$

where *x* was varied from 0.0 to 0.8 in each series.

The template tetrapropylammonium bromide (TPABr) as well as *n*-propyl amine as a mobilizing agent were mixed together with the sodium silicate and added to a clear solution of aluminum sulfate (~5 ml). Solution of a calculated amount of $Fe(NO_3)_3$ was added dropwise to the previous solution simultaneously with constant stirring for 30 min. The pH of the mixture was adjusted to 11.0 by using sulfuric acid (0.1 M) or sodium hydroxide (0.1 M). The amorphous gel was formed and allowed to age for 1 h at room temperature. The reaction mixture was transferred to 300 ml stainless steel autoclaves and maintained in an oil bath at 160 °C under autogenously pressure. The autoclave was removed from the oil bath after 8 days and quenched in cold water for product identification. The solid products were separated by filtration. Excess alkali was thoroughly washed with water repeatedly until the pH of washing liquid was close to 8, and the products were dried in an oven at 120 °C for 10 h, then calcined at 550 °C for 6 h to remove the template. Its pale brown color was deeper by increase Fe content. All series of samples were prepared from the gels with total $SiO_2/(Al_2O_3 + Fe_2O_3)$ molar ratio of 38. These samples were denoted as 0.2FeZ, 0.4FeZ, 0.6FeZ and 0.8FeZ depend on the ratio of Fe.

2.2. Instrumental techniques

The X-ray diffractograms of various zeolitic samples were measured by using a Philips diffractometer (PW-3710). The patterns were run with Ni-filtered copper radiation (Kα = 1.5404 Å) at 30 kV and 10 mA with a scanning speed of $2\theta = 2.5°$/min. The crystal sizes of the prepared materials were determined using the Scherrer equation. The instrumental line broadening was measured using a LaB_6 standard. The crystallinity of the prepared samples was calculated using the ratio of the sum of the areas of the most intense peaks for modified AlZSM-5 samples ($2\theta = 20–25°$) to that of the same peaks of the prepared AlZSM-5 and multiplying by 100.

The Fourier transform infrared (FT-IR) spectra were recorded on a Jasco FT-IR-40, single beam spectrometer with a resolution of 2 cm^{-1}. The samples were ground with KBr (1:100 ratio) as a tablet and mounted to the sample holder in the cavity of the spectrometer. The measurements were recorded at room temperature in region at 1400–400 cm^{-1}.

UV–vis diffuse reflectance spectra of the samples were measured using a JASCO V-570 unit, serial no. 29635, at scanning speed 4000 nm/mm and a band width 2 nm. The samples were measured in the wavelength range from 200 to 500 nm. The samples were prepared as self-supporting wafers and were recorded at room temperature.

The nitrogen adsorption isotherms were measured at −196 °C using a conventional volumetric apparatus. The specific surface area was obtained using the BET method. The micropore volume and the external surface area were obtained from the *t*-plot method.

Chemical composition of rice husk ash was examined by X-ray fluorescence spectroscopy (XRF: Philips, PW1400).

2.3. Catalytic activity

2.3.1. Determination of PNP

The concentration of PNP was measured by UV spectrophotometer JASCO V-570 unit, serial no. 29635. After illumination, clear samples were obtained by filtering the solution using Millipore filter (0.45 μm), then adjusted pH, used for the analysis of PNP by measuring the absorbance at 400 nm.

2.3.2. Photocatalytic degradation experiment

The photoreactivity experiments were carried out in a cylindrical Pyrex glass reactor containing 0.20 g of catalyst and 250 ml of aqueous solution of *p*-nitrophenol (PNP). The concentration of the

organic compound was 5×10^{-3} M. Prior to irradiation, after adjusting pH, the suspensions were magnetically stirred in the dark for 60 min to establish the adsorption/desorption equilibrium of the PNP. The aqueous suspensions containing PNP were irradiated with constant aerating. At given irradiation time intervals, samples were taken from the suspension, and then passed through a 0.45 μm Millipore filter to remove the particles; the concentration of PNP in the filtrate was measured by applying the following equation.

$$\%\ \text{removal efficiency} = \frac{C_0 - C}{C_0} \times 100$$

where C_0 is the original *p*-nitrophenol (PNP) content and C is the retained PNP in solution.

3. Results and discussion

3.1. X-ray diffraction

X-ray diffraction (XRD) patterns of iron substituted ZSM-5 and parent ZSM-5 samples (Fig. 1) showed typical lines of the parent aluminosilicate ZSM-5 synthesized using TPABr template, indicating the intact structure of ZSM-5 even after incorporation of Fe ions. Fe-ZSM-5 samples showed small particles at d = 5.3497, 4.696, 4.469, 4.07363, 3.712, 3.339, 2.9426 and 1.5996 Å related to iron silicate phase. However, the samples (0.6Fe and 0.8Fe) containing high lodging iron substitution were well crystalline, and a few of α-Fe_2O_3 phase which were hardly recognized as small particles at d-spacings = 3.67, 2.42, 2.20 and 1.69 Å, respectively [25].

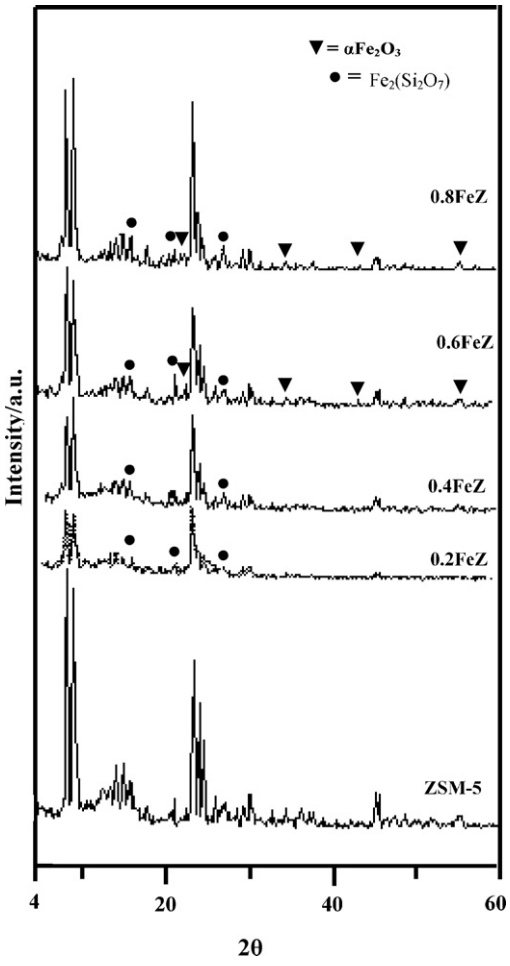

Fig. 1. X-ray powder diffraction patterns of ZSM-5, 0.2FeZ, 0.4FeZ, 0.6FeZ and 0.8FeZ.

Table 1
Effect of iron substituted Al in ZSM-5 on the particles size and unit cell parameters of the synthesized ZSM-5 zeolite.

Samples	D (Å)	Unit cell (Å)			Cell volume (Å)^3	Crystallinity %
		a	b	c		
Al-ZSM-5	99.28	19.652	19.818	13.363	5204.440	100
0.2Fe	86.16	19.920	19.906	13.345	5291.659	76
0.4Fe	72.18	20.259	20.010	13.380	5424.019	69
0.6Fe	60.24	19.735	19.558	13.370	5160.252	60
0.8Fe	75.96	19.812	19.501	13.315	5144.037	83

Note: a, b and c are the lattice parameters (Å), V is the lattice volume (Å)^3; $a \times b \times c$. D is the particles diameter (Å). The crystallinity of the prepared samples was calculated using the ratio of the sum of the areas of the most intense peaks for modified AlZSM-5 samples (2θ = 20–25°) to that of the same peaks of the prepared AlZSM-5 and multiplying by 100.

The effect of Fe loadings on crystallinity percentages, crystallites size, unit cell parameters and cell volume of ZSM-5 zeolite were depicted in Table 1. A monotonous decrease in crystallinity for 0.2FeZ and 0.4FeZ samples was observed (76% and 69%, respectively). This decreasing was in line with increasing the lattice volume of the same samples when compared with that of the parent pointing together to the presence of some Fe species in a highly dispersed state inside zeolite channels. The recognized increase in lattice volume was due to increasing the accessibility of Fe ions into ZSM-5 channels specifically in tetrahedral positions. The value of the average crystal size of ZSM-5 calculated by Scherrer equation for 0.2FeZ and 0.4FeZ samples were found to be 86.16 and 72.18 nm, respectively, and thus representing the lowest crystal size of all samples. This demonstrates that incorporating Fe in ZSM-5 effectively prevent particle agglomeration, of this particular sample (0.4FeZ), allowing the material to maintain its dispersion. Accommodating small Fe particles in micropores can also cause expansion in unit cell and pore volume.

On the other hand, the 0.6FeZ and 0.8FeZ samples presented the lowest lattice volume between all samples giving a criterion about decreasing the diffusion of Fe ions to proceed into compensating positions inside ZSM-5 channels. Accordingly, this sample showed intensified lines of α-Fe_2O_3 species; when compared with the other samples 0.2FeZ and 0.4FeZ, which more or less comparable to the one devoted for 0.2FeZ (30%). Given that the strongest lines of ZSM-5 (2θ = 20–25°) are enhanced in 0.8Fe, hence the diffusion of Fe ions did not take place inside zeolite channels otherwise a relative decrease in crystallinity could have been obtained as conceived for 0.2FeZ and 0.4FeZ samples. Thus, the increase in crystallinity of the former sample could be caused by the presence of iron silicate [$Fe_2(Si_2O_7)$] phase that have lines superimposed those of ZSM-5.

3.2. Framework structure

IR spectra of zeolite lattice vibration modes and the corresponding Fe containing ones are depicted in Fig. 2 in the mid (1400–400 cm^{-1}) range. All spectra of the samples show a typical ZSM-5 structure associated with minor changes because of Fe incorporation. The absorption bands at 1221 and 1095 cm^{-1} correspond to TO_4 asymmetric stretching vibration, while the other bands at 792, 546 and 453 cm^{-1} correspond to TO_4 symmetric stretching, double ring and bending vibrations, respectively [4,23,24]. With the increase of the Fe/Al ratio the absorption bands at 1221 (1232) and 1095 (1008) cm^{-1} shifted to lower wave numbers which suggests the good incorporation of Fe species inside ZSM-5 zeolite channels, most likely in compensating positions [4].

Of particular importance, the internal asymmetric stretching vibration of Si–O–T observed at 1095 cm^{-1}, for aluminosilicate (parent ZSM-5), show splitting in the higher Fe substitution Al in ZSM-5 into 1103 cm^{-1} besides the permanent existence of the one

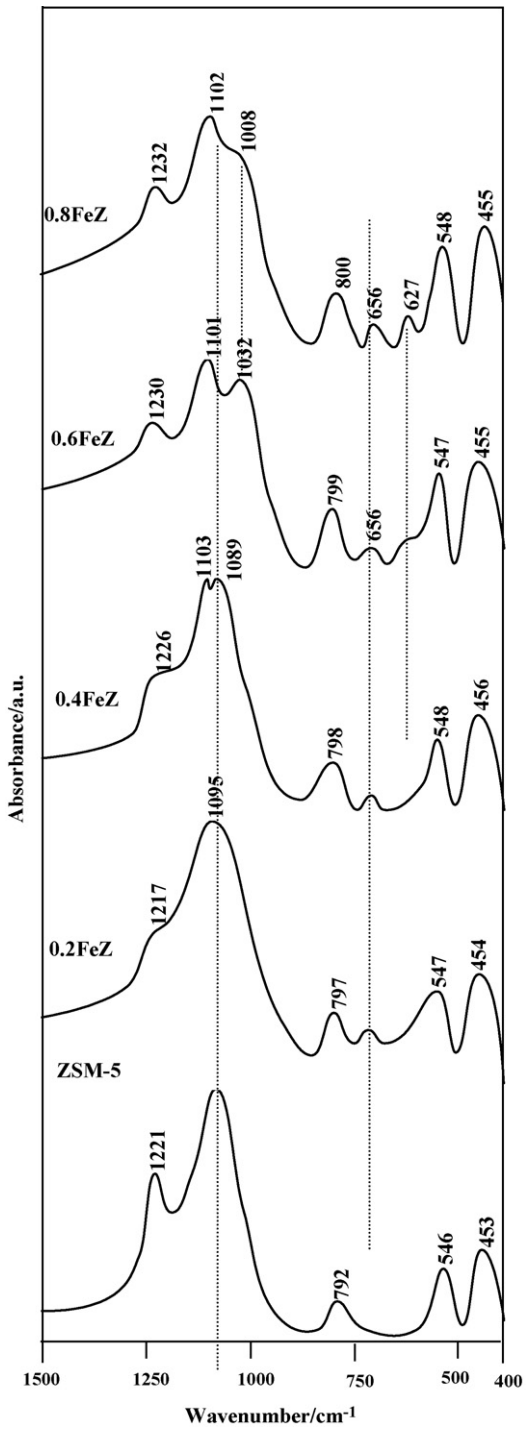

Fig. 2. FT-IR absorbance spectra of ZSM-5, 0.2FeZ, 0.4FeZ, 0.6FeZ and 0.8FeZ.

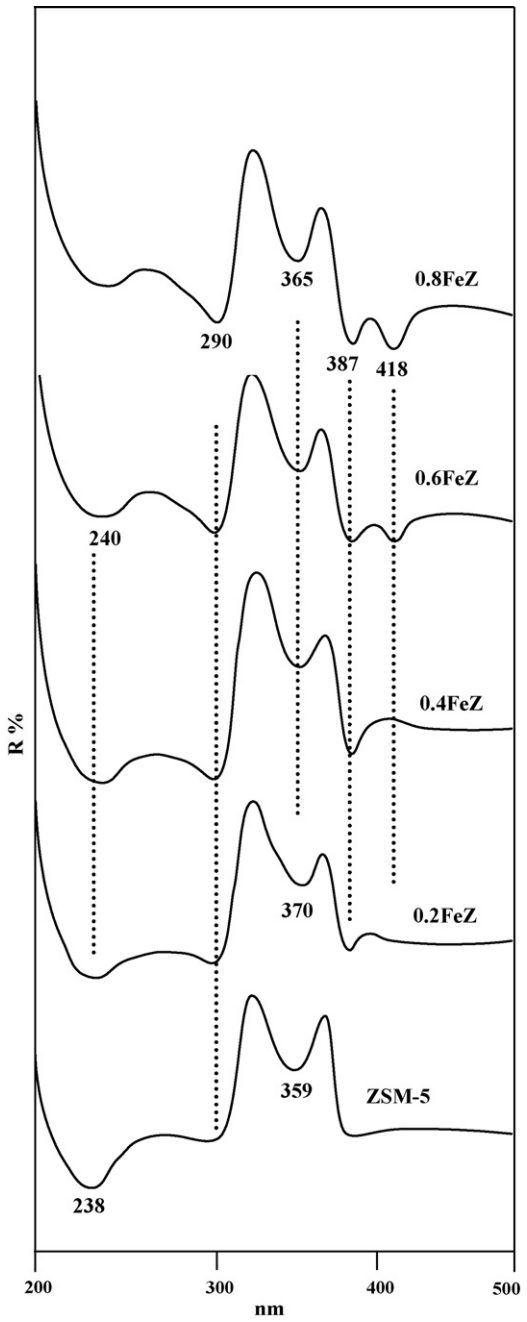

Fig. 3. UV–vis absorption spectra of ZSM-5, 0.2FeZ, 0.4FeZ, 0.6FeZ and 0.8FeZ.

at 1008 cm^{-1}. This could be due to the presence of residual Al^{3+} nearby Fe^{3+} in the same site. Based on the values of the percentages of the ionic character of Fe–O and Al–O linkages that equal 54 and 64, respectively, a more covalent character of the former is indeed expected that have a superior electronegativity (1.64 vs. 1.47) as well [4].

The new band at 656 cm^{-1} appeared in all samples (Fe-substituted zeolite) may be ascribed to symmetric stretching to Si–O–Fe [26]. This band did not exist in the parent sample. This band showed an increased intensity because of increasing Fe replacement into ferrisilicate. In the other hand new band appeared at high Fe substitution (0.6FeZ and 0.8FeZ) at 627 cm^{-1} related to Fe–O vibration mode [27–29].

3.3. UV–vis diffuse reflectance spectroscopy

The UV–vis diffuse reflectance spectra measured at room temperature for all Fe-substituted and parent ZSM-5 samples shown in (Fig. 3) were recorded in order to obtain some information about their electronic properties. The parent ZSM-5 showed two bands at 238 and 359 nm. The band appear at 359 nm is related to T_2 transition which is assigned to Al–O units characterized by a highly charged oxygen atom and a highly electron-deficient aluminum atom compared to that of Al-units of the T_1 transition (238 nm) charge-transfer processes [30].

Table 2
Some surface characteristics of ZSM-5 and iron substituted Al in ZSM-5 investigated adsorbents; prepared by different methods, heating at 300 °C under a reduced pressure of 10^{-5} Torr.

Samples	SBET (m^2/g)	S_t (m^2/g)	S^{μ} (m^2/g)	S^{ext} (m^2/g)	S^{wid} (m^2/g)	r^- (Å)	V_p^{total} (cm^3/g)	V_p^{μ} (cm^3/g)	V_p^{wid} (cm^3/g)
Al-ZSM-5		658	593	115	67	21.0	0.554	0.498	0.056
0.2Fe	737	753	662	80	75	23.3	0.688	0.617	0.0702
0.4Fe	846	840	788	75	56	20.0	0.696	0.651	0.0444
0.6Fe	721	730	672	69	49	21.3	0.614	0.572	0.042
0.8Fe	650	641	541	73	109	23.4	0.609	0.507	0.102

Note: (S_{BET}) BET-surface area; (S_t) surface area derived from V_{1-t} plots; (S^{ext}) externalsurface area; (S^{μ}) surface area of micropores; (S^{wid}) surface area of wide pores; (V_p^{total}) total pore volume; (V_p^{μ}) pore volume of micropores; (r^-) mean pore radius.

The UV–vis reflectance spectra of Fe-ZSM-5 samples showed absorption bands at 240, 310, 356 and 387 nm observed for all Fe containing ZSM-5 samples. A band at 418 nm also viewed for high Fe/Al ratio in Fe-ZSM-5 samples. The charge-transfer bands ($Fe^{3+} \leftarrow O$) at 240 ($\lambda < 300$ nm) and 290 nm are typically attributed to isolated Fe^{3+} species, either tetrahedrally coordinated in the zeolite framework or with high coordination [31]. A broad band at 418 nm characteristic of Fe^{3+} ions present as α-Fe_2O_3 nanoparticles at the external surface of the zeolite crystals ($\geq$400 nm) were depicted. The band at 387 nm assigned to iron ions in small oligonuclear clusters [32] were enhanced in high Fe substitution probably at the expense of that at 418 nm. This might be due to dislodgment of framework Fe^{3+} ions and even a certain degree of Fe association. The presence of a broad band at 418 nm in high Fe-substituted (0.6FeZ and 0.8FeZ) indicates that α-Fe_2O_3 particles are formed as a result of partial removal of Fe from framework positions.

It is noteworthy mentioning that the color of the samples is still in contact even following acid leaching (HCl, 0.1 M, 3 h). This indicates that the majority of Fe species are in tetrahedral positions or in highly dispersed state inside zeolite channels.

3.4. Surface texture

The different surface characteristics of the investigated zeolitic samples were determined and the data obtained is given in Table 2. Inspecting of the data compiled in this table reveals the following: (i) the S_{BET} and S_t of various adsorbents are close to each other which justifies the correct choice of *t*-curve used in analysis and indicate the absence of ultra-microporous; (ii) both S_{BET} and V_p of the investigated zeolite was found slightly increased (28 and 20%), respectively, in the lower substituted Al by Fe (0.2FeZ, 0.4FeZ) but lower with increased substitution (0.6FeZ, 0.8FeZ); (iii) the average pore diameter of ZSM-5 remains almost constant in all prepared solids; (iv) the values of external surface area of the various samples comprise values $\leq$10% of the S_{BET}, indicating the mesoporosity nature of these materials except the parent that measured a value comprises of 17%, reflecting the higher microporosity of this particular sample; (v) decreasing the total pore volume of the samples (0.6FeZ and 0.8FeZ from replaced Al by Fe) when compared with the rest of the samples indicating the probability of presence of Fe species in a separate phases probably as oxides or as iron silicate species.

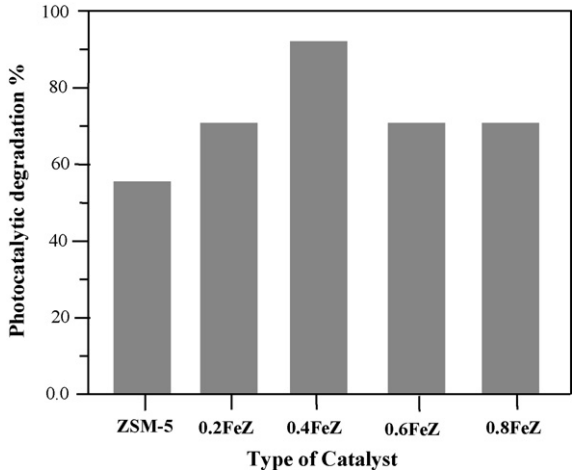

Fig. 4. The efficiency of PNP photodegradation over various catalysts. Experimental conditions: pH 5, reaction volume 250 ml, catalyst content 0.2 g, reaction time 60 min, initial PNP concentration 5×10^{-3} M.

Combining the results obtained from XRD, FT-IR, UV–vis and BET investigations, one may suggest that an increase in lattice volume; lowest crystallites size and maximum S_{BET} in 0.4Fe sample between all samples suggesting the presence of the majority of Fe ions in tetrahedral positions inside zeolite channels. On the other hand, α-Fe_2O_3 species may deposit on the outermost surface layers of the zeolite blocking some pores in 0.6Fe and 0.8Fe samples thus, reducing their surface areas comparatively.

3.5. Photocatalytic activity

The Fe-substituted ZSM-5 has been used as a catalyst in the photocatalytic degradation of *p*-nitrophenol. The iron content was varied from 0.2FeZ into 0.8FeZ in the degradation reaction and showed that Fe containing ZSM-5 at the 0.4FeZ substituted was the most active catalyst (Fig. 4). The samples containing high loading Fe (0.6FeZ and 0.8FeZ) as well as containing α-Fe_2O_3 showed low catalytic activity. This may indicate that Fe is active when incorporated inside zeolite (heterogeneous phase) and its share in the reaction activation may come following that of ZSM-5. On the other hand, charge-transfer process on M–O moieties (of tetrahedral structure) may involve an electron transfer from the O^{2-} to M^+ ions forming charge-transfer excited triple state:

$$M^+ = O^{2-} + h\upsilon \rightarrow (M^{\pm} - O^-)^{\bullet}$$

Thus, adsorption of molecules with electron donating nature and those with electron accepting nature either within zeolite or on its external surface can lead to the CT complexes due to attractive force between the donor–acceptor pairs [23,33]. Thus, a remarkable enhancement in photocatalytic decomposition of PNP is attained by such synergism. This highlights that the photocatalytic oxidation of the PNP on 0.4Fe is primarily due to the charge-transfer relating an electron transfer from the O^{2-} of SiO_4 unit to the coordinated Fe ions.

In order to determine the optimal amount of photocatalyst, a series of experiments with varied amounts of the 0.4FeZ catalyst have been conducted. The amount of the photocatalyst was varied between 0.05 and 0.5 g/dm^3 of 0.4FeZ. The catalyst was added to 250 ml of 5×10^{-3} M PNP, stirred and irradiated them for 60 min. The samples were taken from the suspension, passed through a 0.45 μm Millipore filter to remove the particles, the concentration of PNP in the filtrate was determined at once. The influences of the mass of 0.4FeZ on the degradation efficiency of

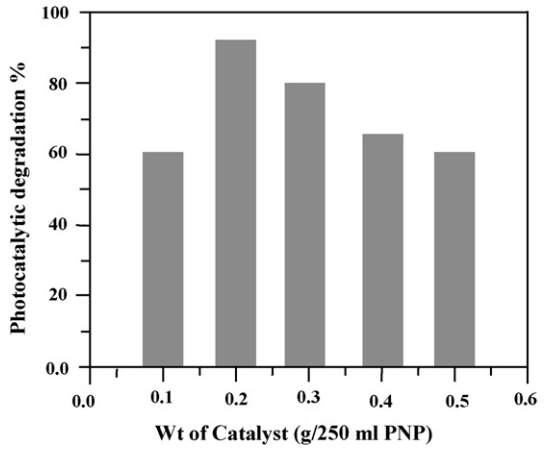

Fig. 5. Effect of photocatalyst content of 0.4FeZ on the decolorization of PNP. Experimental conditions: pH 5, $T = 25\ ^{\circ}C$, time = 60 min, volume = 250 ml, initial PNP concentration 5×10^{-3} M.

PNP are shown in Fig. 5. It was observed that the degree of photocatalytic efficiency of PNP solution increased with increasing the loading catalyst amount, till 0.2 g. The most effective decomposition of PNP (92%) was observed with the catalyst amount equal to 0.2 g after which (0.25–0.5 g of catalyst loading) the photocatalytic efficiency decreases. This phenomenon caused by the so-called shielding effect, i.e. exceeding the optimal amount of the suspended 0.4FeZ particles increases the complex formation with the PNP and thus blocking off the available surface active sites. Increasing the suspended particles of Fe containing zeolites reduced the adsorption from solution due to the expected crowding of the PNP molecules during the adsorption process. Many authors have investigated the reaction rate as a function of catalyst amounts under different experimental conditions [34–38]. They concluded that the increase of catalyst amounts promote the existence of the presence of parallel paths associated with catalyst degradation during the catalytic cycle (e.g. dimerization reaction) [39], and thus, increases as the concentration of the amount of a catalyst increase. However, attaining complete degradation of the PNP at specific catalyst concentration (0.2 g) nullifies the possibility of the presence of competing paths for the reaction and indeed suggests a facile pathway for degradation of such a PNP.

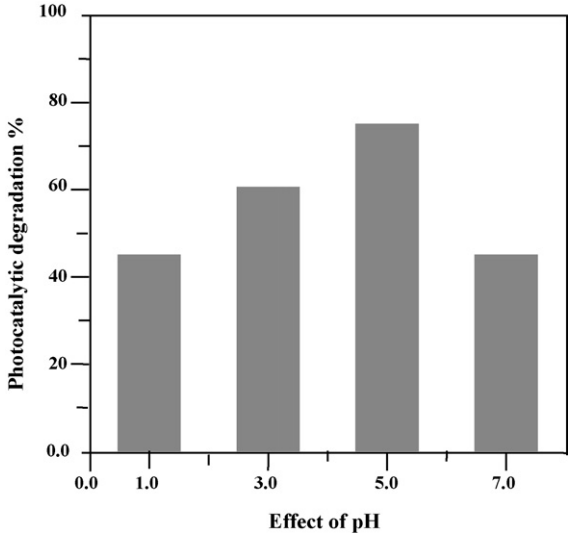

Fig. 6. Effect of pH on the photodegradation percentages of PNP on 0.4FeZ. Experimental conditions: reaction volume 250 ml, catalyst content 0.2 g, reaction time 60 min, initial PNP concentration 5×10^{-3} M.

The degradation efficiency of PNP on 0.4FeZ at different pH levels was shown in Fig. 6. The pH of the solution was adjusted with dilute NaOH and HCl solutions. The different concentrations of acid or base have been chosen in order to add the minimum quantity of these species to avoid the volume change of the reaction mixture. It was found that the degradation of PNP over 0.4FeZ was highly pH dependent, with the degradation efficiencies increased with decreasing pH values. This is evidence that the contribution of the leaching iron activity to the Fe-ZSM-5 activity in the organic oxidation is negligible all along the catalyst use. Thus, the most part of iron in Fe-ZSM-5 exists in a stable form, does not leach from the catalyst and is active in the organic oxidation by hydrogen peroxide during manifold use of the catalyst. It is likely that this part of iron exists in the framework position of zeolite; however, the role of di-/oligonuclear iron complexes, consisting of the zeolite, in the H_2O_2 decomposition reaction is unclear and cannot revealed from the given experimental data [40]. The main reason of different initial pH values of the suspensions a signed to the content of aluminum also influences the catalyst acidity [41].

4. Conclusions

Silica derived from rice husk ash has been used to synthesize ZSM-5 zeolite with Si/Al ratio of 38. Fe-substituted ZSM-5 has also been hydrothermally synthesized by using TPABr template conditions by replacing Al with Fe at constant $SiO_2/(Al_2O_3 + Fe_2O_3)$ molar ratios.

- The replacement of Al^{3+} by Fe^{3+} with larger ionic radius causes a shift of Si–O–T vibration to lower wavenumbers. The presence of tetrahedral Fe^{3+} has been confirmed by XRD and UV–vis spectroscopy.
- By comparing the lattice volume of the Fe-substituted ZSM-5 samples with that of no iron, one observes that the lattice volume increase in case of 0.2FeZ and 0.4FeZ samples pointing to the presence of some Fe species in a highly dispersed state inside zeolite channels. The recognized increase in lattice volume was due to increasing the accessibility of Fe ions into ZSM-5 channels exchanging Na ions located therein.
- The Fe-substituted ZSM-5 has been used as a catalyst in the photocatalytic degradation of *p*-nitrophenol. 0.4FeZ was found to be the most active sample in the degradation of PNP in accordance with the higher dispersion Fe and larger value of its BET surface area. It seems that the photocatalytic degradation of PNP can be accelerated by various Fe species specifically those in framework positions and those exhibiting finally dispersed Fe_2O_3 species.

References

[1] A.E. Shilov, G.B. Shulpin, Chem. Rev. 97 (1997) 2879.
[2] R.M. Barrer, Hydrothermal Chemistry of Zeolite, Academic Press, London, 1982, p. 251.
[3] W. Peng, T. Komatsu, T. Yashima, Micropor. Mesopor. Mater. 20 (1998) 139.
[4] M.M. Mohamed, I. Othman, N.A. Eissa, Micropor. Mesopor. Mater. 87 (2005) 93.
[5] T.M. Salama, M.M. Mohamed, I. Othman A., G.A. El-Shobaky, Appl. Catal. A 286 (2005) 85.
[6] M.M. Mohamed, T.M. Salama, A.I. Othman, G.A. El-Shobaky, Appl. Catal. A 286 (2005) 85.
[7] Z. Gabelica, S. Valange, Micropor. Mesopor. Mater. 30 (1999) 57.
[8] A.V. Kucherov, A.A. Slinkin, G.K. Beyer, G. Borbely, J. Chem. Soc., Faraday Trans. 85 (1989) 2737.
[9] T. Inui, D. Medhanavyn, A. Miyamoto, React. Kinet. Catal. Lett. 34 (1987) 69.
[10] N.K. Mal, A. Bhaumik, V. Ramaswamy, A.A. Belhekar, A.V. Ramaswamy, Stud. Surf. Sci. Catal. 94 (1995) 317.
[11] A. Hagen, K.H. Hallmeier, C. Hennig, R. Szargan, T. Inui, F. Roessner, Stud. Surf. Sci. Catal. 94 (1995) 195.
[12] L. Brabec, M. Jeschke, R. Klik, J. Novakova, L. Kubelkova, J. Meusinger, Appl. Catal. 170 (1998) 105.
[13] P. Fejes, J.B. Nagy, K. Lazar, J. Halasz, Appl. Catal. Part A: Gen. 190 (2000) 117.
[14] G.J. Kim, W.S. Ahn, Appl. Catal. 71 (1991) 55.
[15] M.A. Uddin, T. Komatsu, T. Yashima, J. Catal. 150 (1994) 439.

[16] M.A. Uddin, T. Komatsu, T. Yashima, Chem. Lett. (1993) 1037.
[17] M. Rauscher, K. Kesore, R. Monning, W. Schwieger, A. Tibler, T. Turek, Appl. Catal. Part A: Gen. 184 (1999) 249.
[18] V.I. Sobolev, G.I. Panov, A.S. Kharitonov, V.N. Romannikov, A.M. Volodin, K.G. Lone, J. Catal. 139 (1993) 435.
[19] A.S. Kharitonov, G.A. Sheveleva, G.I. Panov, V.I. Sobolev, Y.A. Pauskhtis, V.N. Romannikov, Appl. Catal. 98 (1993) 33.
[20] L.J. Lobree, I.C. Hwang, J.A. Reimer, A.T. Bell, J. Catal. 186 (1999) 242.
[21] E.M. El-Malki, R.A. van Santen, W.M.H. Sachtler, J. Catal. 196 (2000) 212.
[22] R.W. Benjamin, A.R. Jeffrey, T.B. Alexis, J. Catal. 209 (2002) 151.
[23] M.M. Mohamed, F.I. Zidan, M. Thabet, Micropor. Mesopor. Mater. 108 (2008) 193.
[24] I. Othman, Mater. Sci. Eng. A 459 (2007) 294.
[25] J. Zhao, Z. Feng, F.E. Huggins, N. Shah, G.P. Huffman, I. Wener, J. Catal. 148 (1994) 194.
[26] T. Inui, H. Nagata, T. Takeguchi, S. Iwamoto, H. Matsuda, M. Inoue, J. Catal. 139 (1993) 482.
[27] L. Yu, L. Zheng, J. Yang, Mater. Chem. Phys. 66 (2000) 6.
[28] X.Q. Xu, H. Shen, J.R. Xu, X.J. Li, Appl. Surf. Sci. 221 (2004) 430.
[29] V.V. Korolev, A.G. Ramazanova, A.V. Blinov, Russ. Chem. Bull. 51 (2002) 2044.
[30] Y. Ding Ma, C. Shu, W. Zhang, X. Zhang, Y. Han, Xu, Xinhe Bao, J. Mol. Catal. A: Chem. 168 (2001) 139.
[31] J. Perez-Ramirez, J. Catal. 227 (2004) 512.
[32] G. Lehmann, Z. Phys. Chem. Neue. Fol. 27 (1970) 279.
[33] S. Dzwigaj, M. Matsuoka, M. Anpo, M. Che, J. Phys. Chem. B 104 (2000) 6012.
[34] R.W. Matthews, Water Res. 24 (1990) 653.
[35] Z. Mengyue, C. Shifu, T. Yaowu, Water Res. 64 (1995) 339.
[36] M.M. Mohamed, I. Othman, R.M. Mohamed, J. Photochem. Photobiol. A 191 (2007) 153.
[37] I. Othman, R.M. Mohamed, I.A. Ibrahim, M.M. Mohamed, Appl. Catal. 299 (2006) 95.
[38] T.M. Salama, I.O. Ali, A.I. Hanafy, W.M. Al-Meligy, Mater. Chem. Phys. 113 (2009) 159.
[39] L. Canali, D.C. Sherrington, Chem. Soc. Rev. 28 (1999) 85.
[40] E.V. Kuznetsova, E.N. Savinov, L.A. Vostrikova, V.N. Parmon, Appl. Catal. B: Environ. 51 (2004) 163.
[41] M.W. Tamele, Discuss. Faraday Soc. 8 (1950) 270.